analytical chemistry

pubs.acs.org/ac Article

Fluorescence-On Imaging of Reticulophagy Enabled by an Acidity-Reporting Solvatochromic Probe

Xiaoxue Zou,[§] Yilong Shi,[§] Shuo Zhang, Jialiang Quan, Jiahuai Han, and Shoufa Han*

Cite This: *Anal. Chem.* 2023, 95, 11499−11509 Read Online

ACCESS | Metrics & More | Article Recommendations | Supporting Information

ABSTRACT: Aberrant autophagy of the endoplasmic reticulum (reticulophagy) is engaged in diverse pathological disorders. Herein, we reported sensitive imaging of reticulophagy with ER-Green-proRed, a diad combining a solvatochromic entity of trifluoromethylated naphthalimide for long-term ER tracking by green fluorescence and an entity of rhodamine-lactam fluorogenic to lysosomal acidity. Stringently accumulated in the ER to give green fluorescence, ER-Green-proRed exhibits robust red fluorescence upon codelivery with the ER subdomain into lysosomes. The relevance of turn-on red fluorescence to reticulophagy was validated by reticulophagy modulated by starvation, reticulophagic receptors, and autophagy inhibition. This imaging method was successfully employed to discern reticulophagy induced by various pharmacological agents. These results show the potential of ER-targeted pH probes, as exemplified by ER-Green-proRed, to image reticulophagy and to identify reticulophagy inducers.

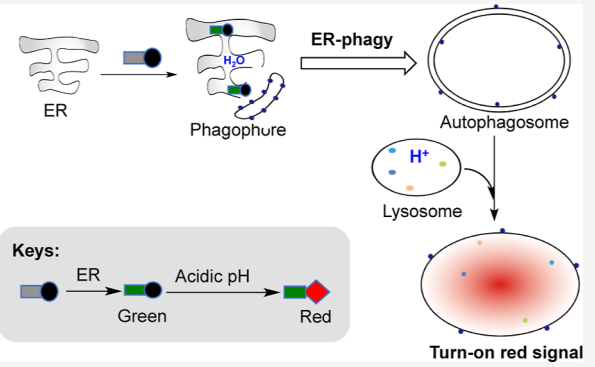

Downloaded via XIAMEN UNIV on February 22, 2024 at 03:00:08 (UTC).
See https://pubs.acs.org/sharingguidelines for options on how to legitimately share published articles.

The endoplasmic reticulum (ER) is the largest membrane-delimited organelle that mediates diverse cell activities ranging from lipid metabolism to ion storage, protein synthesis, folding, and trafficking.[1] A stressed ER plays a causal role in myriad pathological disorders known as ER stress-associated diseases.[2−6] Autophagy is a conserved catabolic mechanism by which superfluous or damaged organelles could be captured and delivered into lysosomes for degradation.[7,8] Given the role of aberrant reticulophagy in ER-stress associated diseases,[2,3,9] methods for reticulophagy imaging are of significance to study reticulophagy[10] and to identify reticulophagy-inducing pharmaceutical compounds.[5]

Reticulophagy has been measured by autophagic degradation of ER proteins[11−13] or with ER-targeted fluorescent proteins.[11,14−16] As overall ER proteins overwhelm the portions degraded in reticulophagy, the former suffers from low sensitivity.[17] Meanwhile, the latter is inapplicable to primary cells and is laborious as it entails plasmid transfection and construction of cell lines expressing protein reporters. In contrast, synthetic small-molecular probes are advantageous in many aspects such as tunable fluorescence and ease of use, representing an attractive modality in bioimaging. Autophagy is hallmarked by the delivery of cargo-enclosed autophagosomes into acidic lysosomes.[18] This process has been employed to detect the autophagy of mitochondria (mitophagy) with mitochondria-targeted pH sensors by sensing lysosomal acidity.[19−43] By contrast, there remains a paucity of suitable small-molecular probes for reticulophagy imaging.[44−49]

We recently reported a rhodol-conjugated pH sensor for reticulophagy imaging by sensing pH acidification in reticulophagy.[46] However, this approach is limited by the always-on green fluorescence of the rhodol entity and susceptibility of probe loss from the ER. To overcome these limitations and to override the need for plasmid transfection and generation of a stable cell line expressing protein reporters, we herein report ER-Green-proRed, a small-molecular probe for long-term high-fidelity imaging of reticulophagy. ER-Green-proRed features an ER-targeting entity with green fluorescence and an entity of X-rhodamine-lactam (ROX-lactam) activable to lysosomal acidity[21,50,51] (Figure 1). Specific for the ER and stably maintained in the ER, ER-Green-proRed allows extended ER tracking by green fluorescence. Upon probe codelivery with ER fragments into lysosomes, ER-Green-proRed is activated by lysosomal acidity to give red fluorescence (Scheme 1), enabling sensitive detection of reticulophagy.

EXPERIMENTAL PROCEDURE

Fluorescence Emission of ER-Green and BZ-ANI at Different Solvent Polarities. ER-Green or Bz-ANI was added to phosphate-buffered saline (PBS) (10 mM, pH 7.5) containing 30, 40, 50, 60, 70, 80, 90, or 100% dioxane (v/v)

Received: May 10, 2023
Accepted: July 3, 2023
Published: July 18, 2023

© 2023 American Chemical Society

https://doi.org/10.1021/acs.analchem.3c02016
Anal. Chem. 2023, 95, 11499−11509

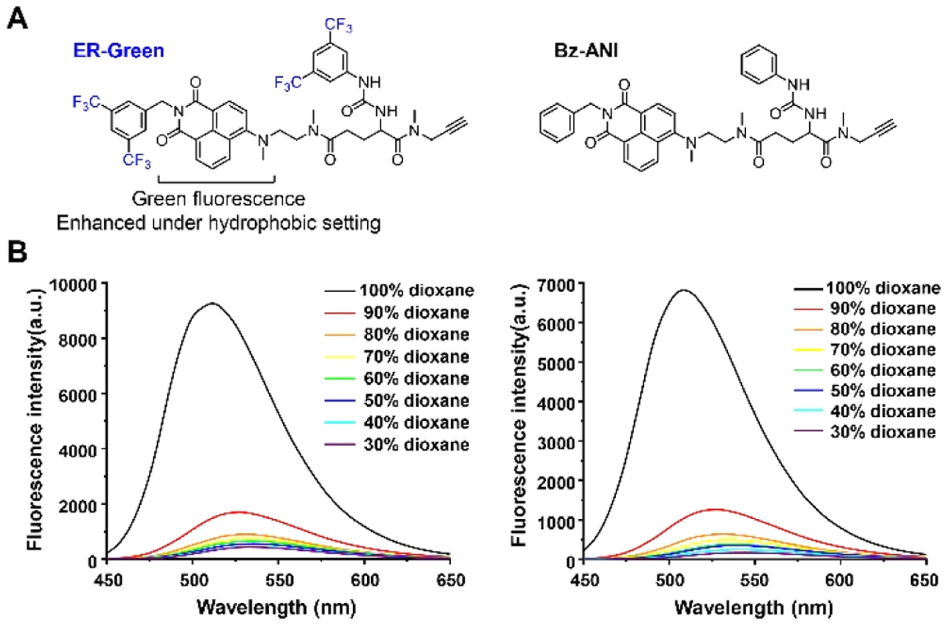

Figure 1. Optical property of ER-Green and Bz-ANI. (A) Chemical structure of ER-Green and Bz-ANI. (B) Polarity-correlated fluorescence emission of ER-Green and Bz-ANI. ER-Green or Bz-ANI was added to phosphate-buffered saline (PBS, 10 mM, pH 7.5) containing 30−100% dioxane to a final concentration of 10 μM. These aqueous samples were analyzed for fluorescence emission using λ_{ex} = 410 nm.

to 10 μM. These aqueous samples were analyzed for fluorescence emission using λ_{ex} = 410 nm.

Selectivity of ER-Green-proRed for the ER. ss-RFP-KEDL$^+$ HeLa cells were stained with ER-Green (5 μM, 1 h), ER-Green-proRed (10 μM, 1 h), or ER-Tracker Green (0.5 μM, 1 h) in DMEM at 37 °C, respectively, and then washed with PBS three times. The cells were analyzed by confocal fluorescence microscopy.

HeLa cells pretreated with ER-Green (5 μM, 1 h) or ER-Green-proRed (10 μM, 1 h) were stained with MitoTracker Deep Red (1 μM, 10 min), LysoTracker Blue (1 μM, 30 min), or Hoechst (2 μg/μL, 20 min) in DMEM at 37 °C, respectively. The cells were rinsed with PBS and then analyzed by confocal microscopy.

ER Targeting in Different Cell Lines with ER-Green. ssRFP-KDEL$^+$ A549 and ssRFP-KDEL$^+$ MCF-7 cells were stained with ER-Green (5 μM, 1 h) at 37 °C, washed with PBS three times, and then visualized by confocal microscopy.

Effects of Trifluoromethyl Moieties of ER-Green on ER Targeting. HeLa cells were stained with ER-Green (5 μM, 1 h) or Bz-ANI (5 μM, 1 h) at 37 °C, washed with PBS three times, and then visualized by confocal microscopy.

Temporal Retention of ER-Green-proRed in the ER. HeLa cells prestained with ER-Green (5 μM, 1 h), ER-Green-proRed (10 μM, 1 h), or ER-Tracker Green (0.5 μM, 1 h) were cultured in fresh DMEM for varied periods of time (0, 1.5, 3, 6, and 10 h). The cells were analyzed by confocal microscopy or flow cytometry.

pH Titration. Fluorescence emission of ER-Green-proRed (10 μM) in PBS (10 mM) containing 30% CH_3OH (pH: 4.0, 4.5, 5.0, 5.5, 6.0, 6.5, 7.0, 7.5, 8.0, 8.5, and 9.0) was collected using λ_{ex} = 410 nm and λ_{ex} = 580 nm.

Cytotoxicity and Fluorescence Yield of ER-Green and ER-Green-proRed. For cytotoxicity, HeLa cells were stained with ER-Green (0, 5, 10, and 20 μM) or ER-Green-proRed (0, 5, 10, and 20 μM) for 1 h and then washed with PBS. The cells were cultured in fresh DMEM for 0, 24, or 48 h and then determined for cell viability and cell number by the cell count kit 8 (MCE, hy-k0301) assay (n = 3).

For the fluorescence yield, ER-Green, Bz-ANI, and ER-Green-proRed were added to dioxane to a final concentration of 10 μM, respectively. The aqueous samples were analyzed for the fluorescence quantum yield using λ_{ex} = 410 nm/λ_{em} = 390−650 nm. ER-Green-proRed was added to PBS (10 mM, pH 4.5) containing 30% CH_3OH to a final concentration of 10 μM. The aqueous sample was analyzed for fluorescence quantum yield using λ_{ex} = 580 nm /λ_{em} = 560−700 nm.

Photostability of ER-Green-proRed In Vitro. ER-Green, ER-Green-proRed, and ER-Tracker Green were dissolved in PBS (10 mM, pH 7.5) containing dimethyl sulfoxide (DMSO, 30% v/v) to a final concentration of 2 μM. The fluorescence intensity was obtained using λ_{ex} = 410 nm for ER-Green/ER-Green-proRed (Green) and λ_{ex} = 505 nm for ER-Tracker Green. ER-Green-proRed (2 μM) in PBS (10 mM, pH 4.0) containing DMSO (30% v/v) was excited using λ_{ex} = 580 nm for red fluorescence of ER-Green-proRed.

Imaging of Reticulophagy with ER-Green-proRed. ss-GFP-RFP-KDEL$^+$ HeLa cells were incubated in DMEM containing 10% fetal calf serum (control) or HBSS (starvation) for 5 h at 37 °C and then visualized by confocal microscopy.

HeLa cells costained with ER-Green-proRed (10 μM, 1 h) and LysoTracker Blue (1 μM, 30 min) were incubated in DMEM (control) or HBSS (starvation) for 5 h at 37 °C prior to confocal microscopic analysis.

Starvation-Induced Red Fluorescence of ER-Green-proRed in Lysosomes. HeLa cells costained with ER-Green-proRed (10 μM, 1 h) and LysoTracker Blue (1 μM, 30 min) were incubated in DMEM (control) or HBSS (starvation) for 5 h at 37 °C prior to confocal microscopic analysis.

RAW264.7, MCF-7, or A-549 cells were stained with ER-Green-proRed (10 μM) for 1 h at 37 °C, washed with PBS three times, and then maintained in DMEM (control) or HBSS (starvation) for 5 h. The cells were analyzed by confocal microscopy.

https://doi.org/10.1021/acs.analchem.3c02016
Anal. Chem. 2023, 95, 11499−11509

Scheme 1. Signal-On Imaging of Reticulophagy with ER-Green-proRed[a]

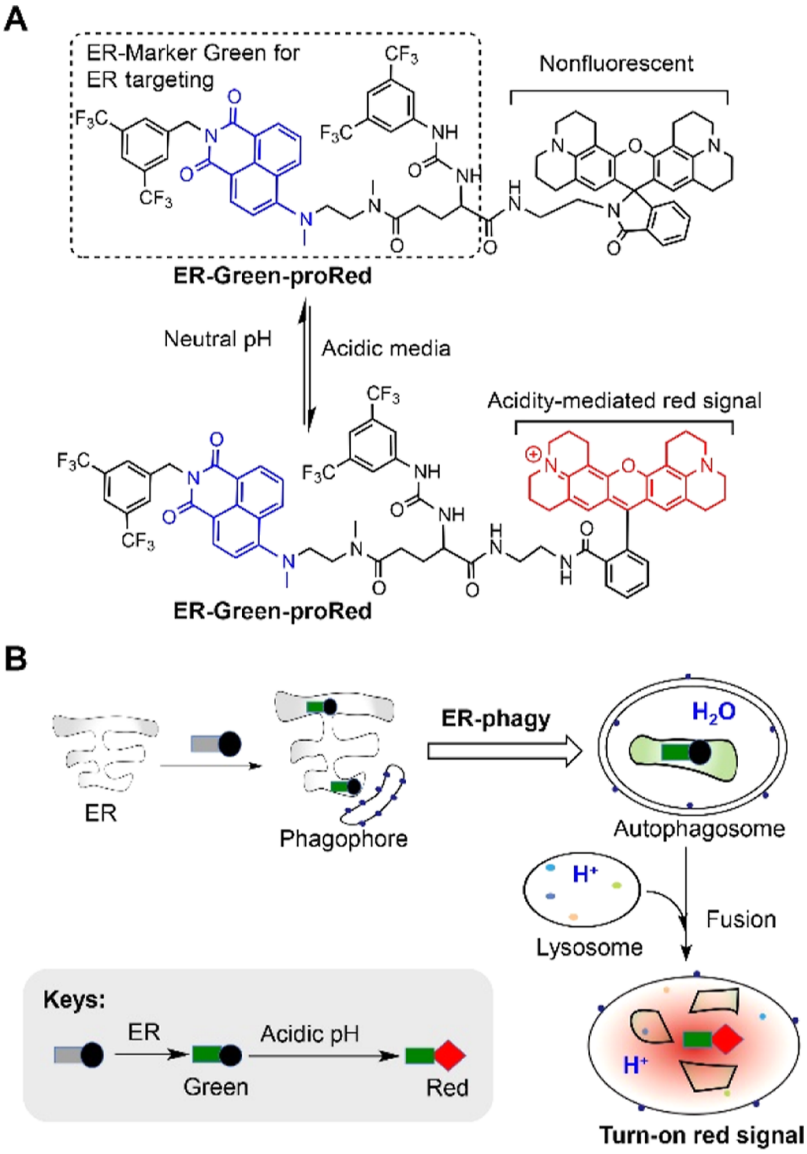

[a](A) Proton-triggered fluorogenic isomerization of ER-Green-proRed gives a rhodamine species of intense red fluorescence. (B) Schematic for reticulophagy imaging with solvatochromic acidity-reporting ER-Green-proRed. Displaying green fluorescence in the ER, the probe gives red fluorescence upon its codelivery with ER fragments into acidic lysosomes in reticulophagy.

Acidity-Mediated Reticulophagy-Reporting Signals. HeLa cells were stained with ER-Green-proRed (10 μM) for 1 h at 37 °C, washed with PBS three times, and then maintained in HBSS or HBSS containing Baf-A1 (25 nM) or CQ (10 μM) for 5 h. The cells were analyzed by confocal microscopy or flow cytometry.

Reticulophagy Receptors Enhance the Optical Activation of ER-Green-proRed. Wild-type (WT), HA-FAM134B$^+$, and HA-TEX264$^+$ HeLa cells were incubated with ER-Green-proRed (10 μM, 1 h) at 37 °C, respectively, incubated in fresh DMEM for 6 h, and then analyzed by confocal microscopy or flow cytometry.

Detection of Small-Molecule-Induced Reticulophagy with ER-Green-proRed in Live Cells. MCF-7 cells were treated with cisplatin (10 μM), CPA (10 μM), etoposide (10 μM), thapsigargin (1 μM), oligomycin (4 μM), rapamycin (3 μM), sodium butyrate (10 mM), or no addition (control) for 24 h and then cultured with ER-Green-proRed (10 μM, 1 h). The cells were washed with PBS three times and then maintained in fresh DMEM for 6 h before confocal microscopy and flow cytometry analysis.

RESULTS AND DISCUSSION

Preparation and Characterization of ER-Green. We sought to develop ER-targeted pH probes to image reticulophagy via sensing pH acidification en route delivery of ER fragments into acidic lysosomes. This necessitates an ER-specific probe that is amenable for further elaboration. Although the mechanism remains to be elucidated, a number of monofluorinated dyes have been documented for ER imaging.[52−60] To test the efficacy of 3,5-trifluoromethylbenzene to target the ER, we combined 3,5-trifluoromethylbenzene and solvatochromic 4-amino-1,8-naphthalimide (ANI) that exhibits green fluorescence substantially enhanced in hydrophobic environments over aqueous media. ER-Green was readily synthesized via a six-step procedure in overall 20% yield

https://doi.org/10.1021/acs.analchem.3c02016
Anal. Chem. 2023, 95, 11499−11509

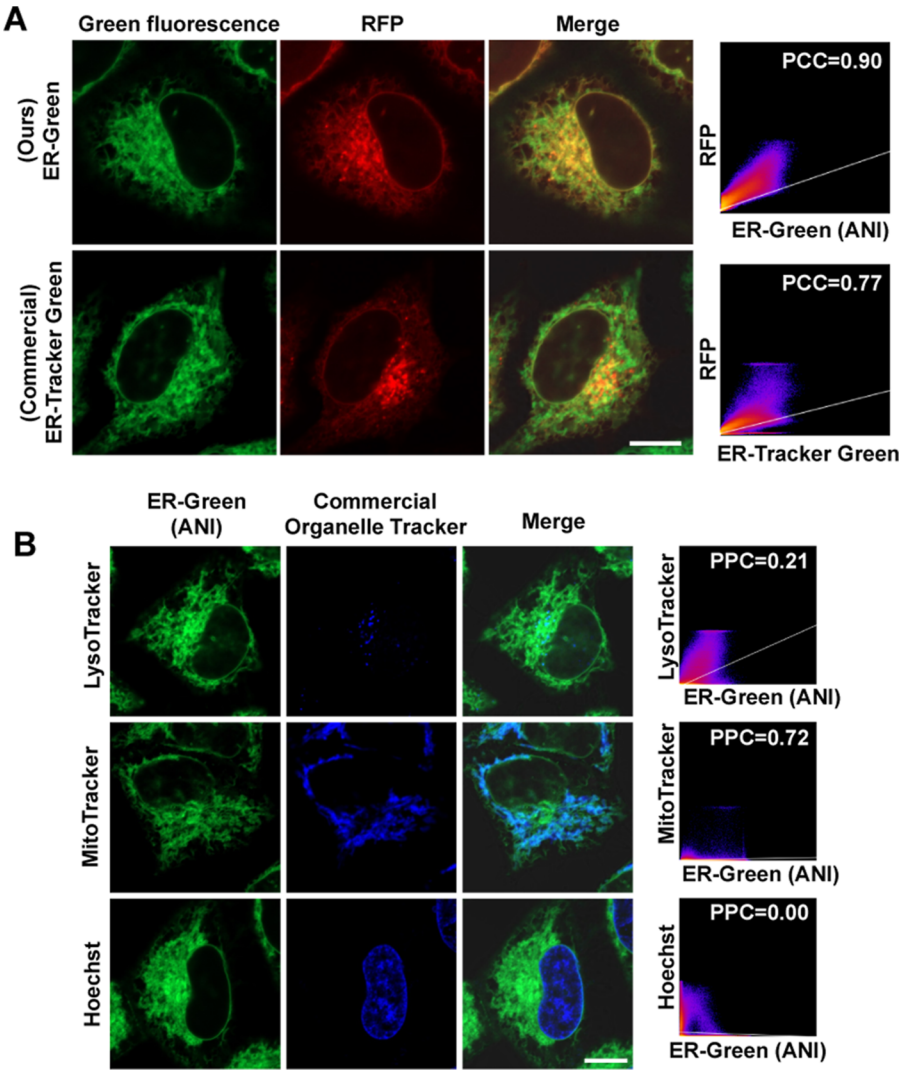

Figure 2. ER imaging with ER-Green. (A) Colocalization of ssRFP-KDEL with ER-Green. ssRFP-KDEL$^+$ HeLa cells were stained with ER-Green (5 μM) or ER-Tracker Green (0.5 μM) for 1 h at 37 °C, washed with PBS three times, and then visualized by confocal microscopy. (B) Selectivity of ER-Green for ER over other organelles. HeLa cells pretreated with ER-Green for 1 h (5 μM) (referred to as ER-Green$^+$ cells) were stained with Hoechst (2 μg/μL, 20 min), LysoTracker Blue (1 μM, 30 min), or MitoTracker Deep Red (1 μM, 10 min), respectively. These cells were rinsed with PBS three times and then visualized by confocal microscopy. Scale bars: 10 μm.

(Scheme S1, Supporting Information). We also prepared Bz-ANI, the structural analogue of ER-Green devoid of the trifluoromethyl moieties. Analysis showed that both ER-Green and Bz-ANI exhibited green fluorescence that increases dramatically in nonpolar medium (dioxane) (Figure 1A,B).

Selective Imaging of the ER with ER-Green. To assess probe selectivity for the ER, ER-Green was applied to HeLa cells expressing ss-RFP-KDEL, a red fluorescence protein (RFP) with N-terminal signal sequence calreticulin (SS) and C-terminal ER retention sequence (KDEL) for targeting and retention in the ER.[61] Confocal microscopic analysis revealed colocalization of ER-Green with ss-RFP-KDEL with a Pearson's correlation coefficient (PCC) of 0.90 (Figure 2A). In contrast, ER-Tracker Green, a commercial dye for the ER, gave a PCC of 0.77 with ss-RFP-KDEL. This showed the superior ER-selectivity of our probe over commercial ER-Tracker Green. Furthermore, ER-Green was largely absent in the lysosomes, mitochondria, and nucleus (Figure 2B). ER-Green also selectively illuminated the ER in ss-RFP-KDEL$^+$ MCF-7 and ss-RFP-KDEL$^+$ A549 cells (Figure S1), showing its applicability in different cell lines. In contrast, no green fluorescence could be observed in cells treated with Bz-ANI under identical assay conditions (Figure S2), showing the critical role of the trifluoromethyl group of ER-Green in targeting the ER and ER-triggered green fluorescence of ER-Green. Combined, these data validate the stringent selectivity of ER-Green for the ER and turn-on green fluorescence ER-Green in the ER.

ER-Green was further evaluated for its temporal retention in cells. HeLa cells prestained with ER-Green or commercial ER-Tracker Green were seeded and incubated in a probe-free culture medium, respectively. Cells were then analyzed by fluorescence microscopy and flow cytometry to quantitate the levels of both probes remaining within cells. This revealed that ER-Green remained detectable at 6 h postincubation, whereas no ER-Tracker Green could be observed at 1.5 h postincubation (Figure 3A−C), showing the superior retention of ER-Green over commercial dyes, indicating its applicability for long-term ER-tracking.

Optical Property of ER-Green-proRed. Encouraged by the stringent selectivity of ER-Green for the ER and its long-

https://doi.org/10.1021/acs.analchem.3c02016
Anal. Chem. 2023, 95, 11499−11509

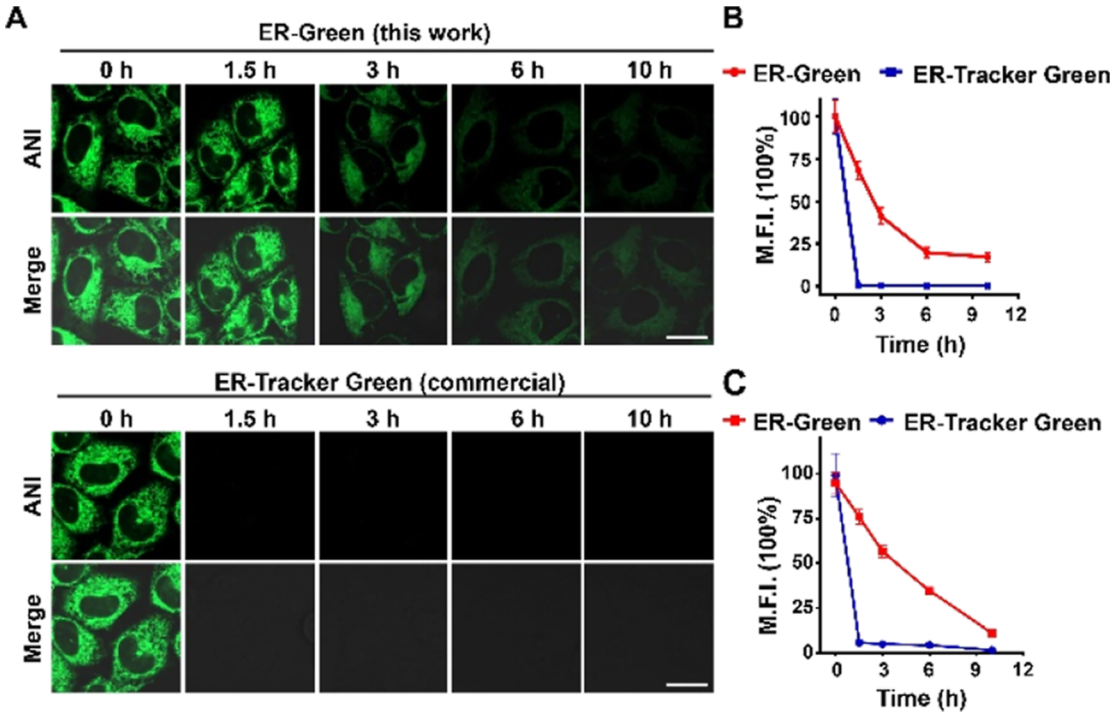

Figure 3. Superior retention of ER-Green in the ER over commercial ER-Tracker Green. ER-Green$^+$ cells or ER-Tracker Green$^+$ cells were cultured in fresh DMEM for varied periods of time and then measured for intracellular fluorescence by confocal microscopy (A,B) or flow cytometry (C). Scale bars: 20 μm. (B) Ten ER-Green$^+$ or ER-Tracker Green$^+$ cells were analyzed by confocal microscopy. The mean intracellular fluorescence intensity (MFI) was plotted over the incubation time. (C) MFI of 10,000 ER-Green$^+$ or ER-Tracker Green$^+$ cells was determined by flow cytometry and then plotted as a function of the incubation time.

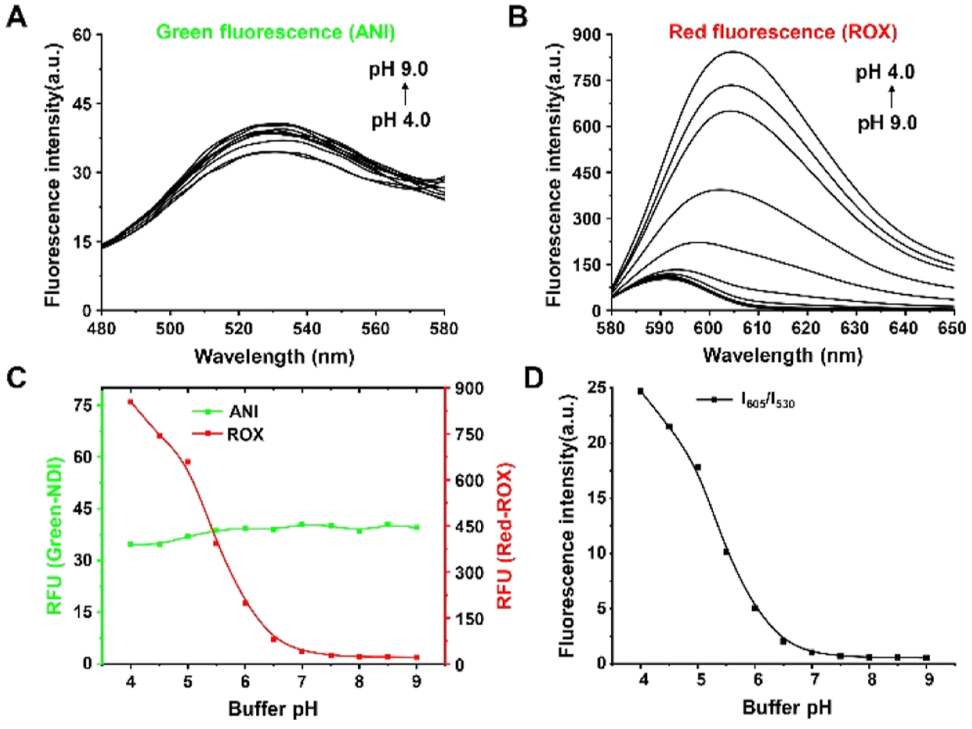

Figure 4. Optical property of ER-Green-proRed. (A,B) Fluorescence emission of ER-Green-proRed. The solution of ER-Green-proRed (10 μM) in PBS (pH 4.0−9.0) was analyzed for fluorescence emission using λ_{ex} = 410 nm for ANI and λ_{ex} = 580 nm for ROX fluorescence. (C) pH titration curve of ER-Green-proRed. The curve was plotted using the fluorescence emission of ANI (I_{530} nm) and ROX (I_{605} nm) over pH. (D) Ratios of red to green fluorescence intensity (I_{605} nm/I_{530} nm).

term retention in the ER, we next coined ER-Green-proRed, a diad consisting of ER-Green for ER targeting and ROX-lactam fluorogenic to acidic lysosomes (Scheme 1A).[21,50,51] After confirming the solvatochromic green fluorescence of ER-Green-

https://doi.org/10.1021/acs.analchem.3c02016
Anal. Chem. 2023, 95, 11499−11509

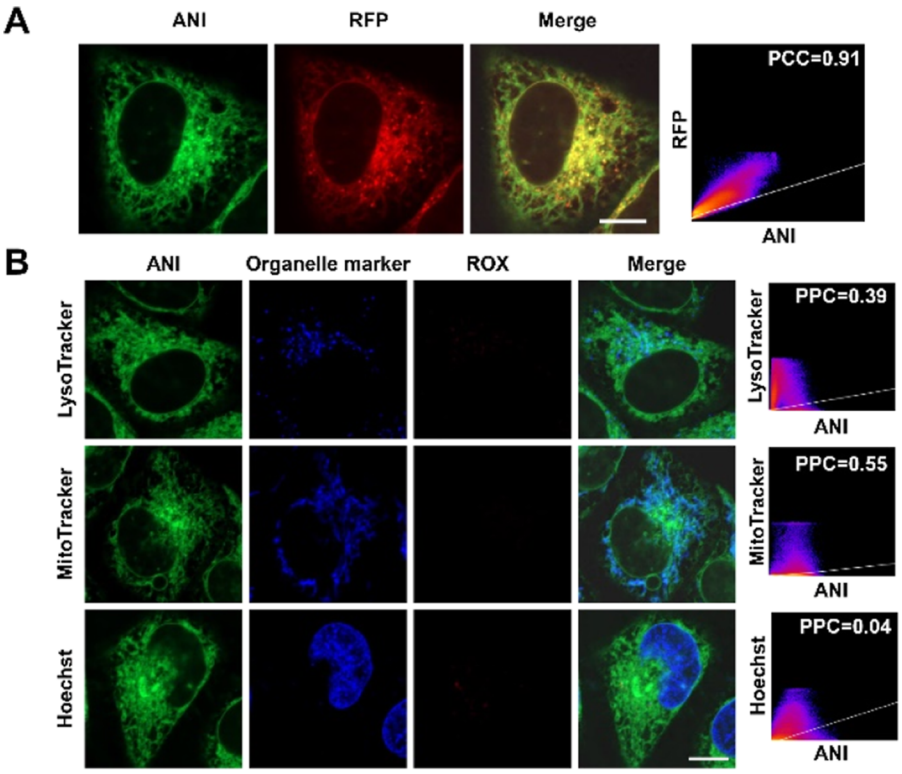

Figure 5. Selectivity of ER-Green-proRed for the ER. (A) Colocalization of ssRFP-KDEL with ER-Green-proRed. ssRFP-KDEL$^+$ HeLa cells were stained with ER-Green-proRed (10 μM) for 1 h at 37 °C before visualization by confocal microscopy. (B) Selectivity of ER-Green-proRed for the ER over other organelles. HeLa cells pretreated with ER-Green-proRed (10 μM, 1 h) were stained with Hoechst (2 μg/μL, 20 min), LysoTracker Blue (1 μM, 30 min), or MitoTracker Deep Red (1 μM, 10 min), respectively. The cells were visualized by confocal microscopy. Scale bars: 10 μm.

proRed akin to that of ER-Green (Figure S3), we assessed its pH responsiveness by measuring the fluorescence emission of ER-Green-proRed in buffer with a pH of 4.0−9.0. As expected, the green fluorescence was largely inert to pH variation, whereas red fluorescence generated in acidic media intensified as the pH decreased. The turn-on red fluorescence was consistent with the protonation-elicited fluorogenic isomerization of ROX-lactam (Figure 4B). ER-Green-proRed exhibited optimal fluorescence emission in the range of pH 4−5 (Figure 4C,D), the window of lysosomal acidity, supporting turn-on red fluorescence upon probe delivery into lysosomes.

Selectivity of ER-Green-proRed for the ER. We applied ER-Green-proRed to HeLa cells and observed bright green signals inside cells but not red signals (Figure 5). The null red fluorescence is consistent with the nonfluorescent state of ROX-lactam of ER-Green-proRed in the ER (Scheme 1). To verify its subcellular distribution, ER-Green-proRed was administered to ss-RFP-KDEL$^+$ HeLa cells. This revealed colocalization of ER-Green-proRed with ss-RFP-KDEL with a Pearson's correlation coefficient (PCC) of 0.91 (Figure 5A). Furthermore, we observed no detectable ER-Green-proRed in the lysosomes (PPC = 0.39 with LysoTracker Blue), mitochondria (PPC = 0.55 with MitoTracker DeepRed), and nucleus (PCC = 0.04 with Hoechst) (Figure 5B). These results demonstrated a high selectivity of ER-Green-proRed for the ER.

Next, the cytotoxicity of ER-Green-proRed was evaluated on HeLa cells. Akin to ER-Green, no detrimental effects on cell viability were observed at a concentration two-fold greater than that used for ER staining (Figure S4). Moreover, time course analysis showed that ER-Green-proRed was effectively retained in cells over the incubation time in a way similar to the ER (Figure S5). In addition, ER-Green-proRed exhibits a green fluorescence yield of 38% in dixoane and a red fluorescence yield of 78% in acidic medium (Figure S6). Finally, HeLa cells stained with ER-Green-proRed or ER-Tracker Green were exposed to constant laser illumination. The intracellular fluorescence intensity was monitored over time by fluorescence microscopy. This showed that the intracellular fluorescence of ER-Tracker Green quickly decayed in 25 min, while ER-Green-proRed exhibited higher levels of green fluorescence emission (Figure S7). Combined, these results indicate the applicability of ER-Green-proRed for long-term live cell ER imaging.

Lysosome-Activated Red Fluorescence of ER-Green-proRed in Starved Cells. We were keen to assess ER-Green-proRed for reticulophagy detection. As reticulophagy could be induced by amino acid starvation,[9,10] HeLa cells prestained with ER-Green-proRed were starved in Hanks' balanced salt solution (HBSS) free of amino acids for 5 h to trigger reticulophagy. For comparison, we also starved HeLa cells expressing ssGFP-RFP-KDEL,[5,14] a ratiometric protein reporter exhibiting enhanced red-to-green emission at acidic settings. We observed massive red puncta across ssGFP-RFP-KDEL$^+$ cells independent of starvation and a moderate increase in red-to-green fluorescence ratios upon starvation (Figure 6A), showing its intrinsic low sensitivity to detect reticulophagy. In contrast, bright red signals were generated in ER-Green-proRed$^+$ cells upon starvation (Figure 6B). In parallel, we performed WB analysis and found that LC3-I and LC3-II decreased in these starved cells (Figure S8). This validated starvation-triggered autophagy. Statistical analysis showed that red fluorescence is 20-fold higher in starved cells than in control cells (Figure 6C), consolidating the high sensitivity of ER-Green-proRed for reticulophagy detection.

https://doi.org/10.1021/acs.analchem.3c02016
Anal. Chem. 2023, 95, 11499−11509

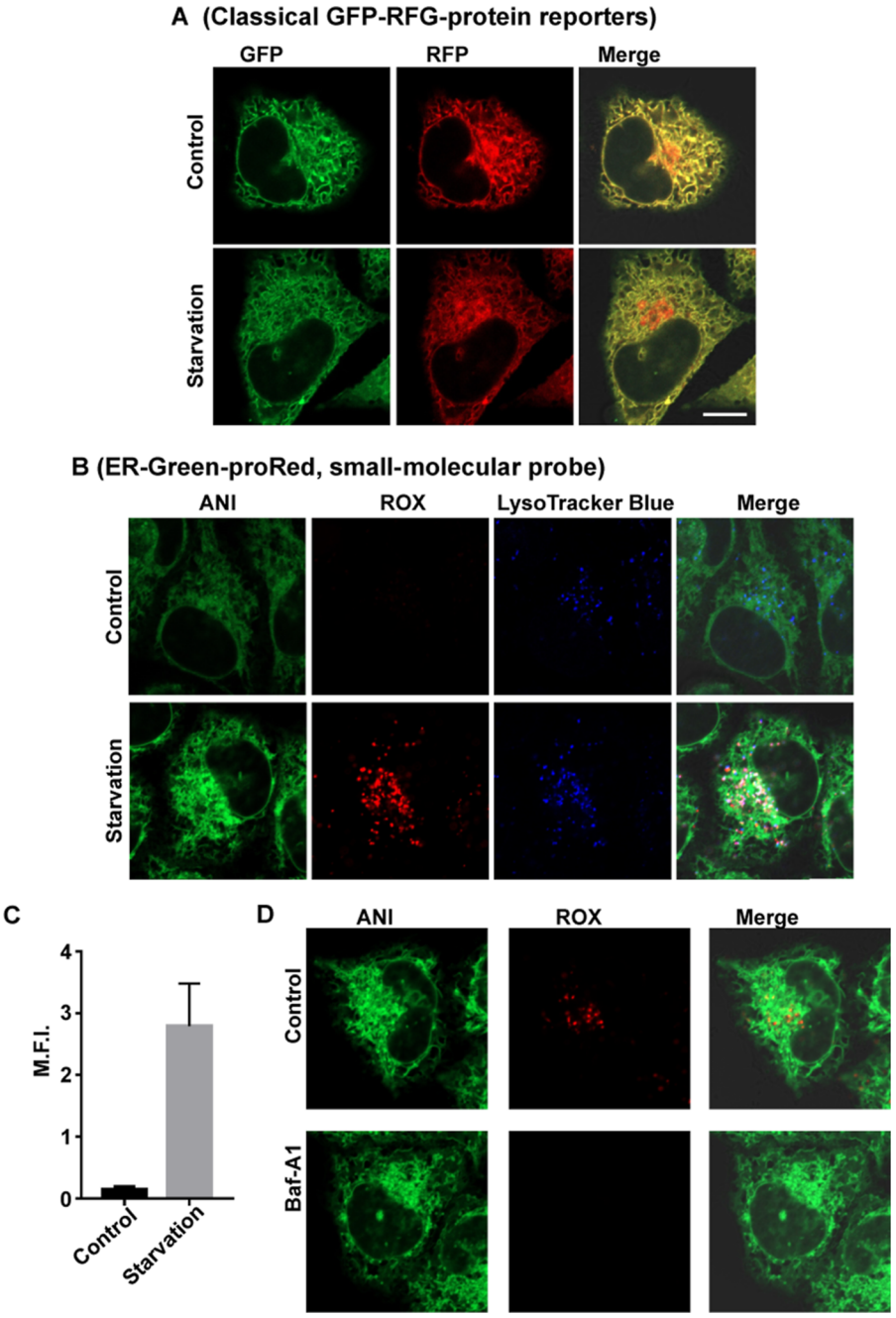

Figure 6. Fluorescence-on imaging of starvation-induced reticulophagy with ER-Green-proRed. (A) Reticulophagy imaging with a fluorescent protein reporter. ss-GFP-RFP-KDEL$^+$ HeLa cells were incubated for 5 h in DMEM (control) or HBSS (starvation) and then visualized by confocal microscopy. (B) Fluorescence-on imaging of reticulophagy with ER-Green-proRed. HeLa cells costained with ER-Green-proRed (10 μM, 1 h) and LysoTracker Blue (1 μM, 30 min) were incubated for 5 h in DMEM (control) or HBSS prior to confocal microscopic analysis. (C) Quantitation of red fluorescence in ER-Green-proRed$^+$ cells before and after starvation. Fluorescence intensity per cell was quantified by ImageJ. mean ± SD, $n = 20$. ****, $P < 0.0001$ (t-test). (D) Lysosomal acidity-mediated turn-on red fluorescence in ER-Green-proRed$^+$ cells upon starvation. ER-Green-proRed$^+$ HeLa cells were incubated for 5 h in HBSS supplemented with Baf-A1 (25 nM) or no addition (control). These cells were analyzed by confocal microscopy. Scale bar: 10 μm.

The response of ER-Green-proRed to starvation-induced reticulophagy was also confirmed in diverse cell lines, including A-549, MCF-7, and RAW264.7 (Figure S9).

We also validated colocalization of the red dots in ER-Green-proRed$^+$ cells with LysoTracker Blue (Figure 6B), a dye specific for lysosomes, reflecting probe delivery into lysosomes and genesis of red fluorescence thereby. We then treated starved ER-Green-proRed$^+$ cells with Bafilomycin A1 (Baf-A1), which effectively neutralizes lysosomes.[62] Baf-A1 caused loss of red fluorescence (Figure 6D), cementing the lysosomal acidity-triggered intense red fluorescence of ER-Green-proRed in lysosomes. Combined, these results show the reticulophagy-mediated delivery of ER-Green-proRed with ER subdomains into acidic lysosomes, whereby the probe is activated by lysosomal acidity to give intense red fluorescence, supporting the use of turn-on red fluorescence as a read-out of reticulophagy.

https://doi.org/10.1021/acs.analchem.3c02016
Anal. Chem. 2023, 95, 11499−11509

Reticulophagy-Dependent Red Fluorescence of ER-Green-proRed in Live Cells. To further validate the dependence of red fluorescence on reticulophagy, ER-Green-proRed$^+$ cells were starved in HBSS supplemented with chloroquine diphosphate (CQ). No red fluorescence could be identified in starved cells treated with CQ (Figure 7). As CQ prevents binding of autophagosomes to lysosomes,[63] failed probe activation in these cells is ascribed to the blockade of ER-Green-proRed into lysosomes by CQ. FAM134B and TEX264 are ER-resident membrane receptors engaged in selective reticulophagy.[9,13,14] As overexpression of FAM134B or TEX264 has been reported to induce reticulophagy[64] and to further verify the relevance of ER-Green-proRed to reticulophagy, we overexpressed HA-FAM134B and HA-TEX264 in HeLa cells, respectively. Both cell samples were stained with ER-Green-proRed and then maintained in fresh cell culture medium for 6 h to allow basal reticulophagy. Null at the initial stage of cell culturing, strong red signals were identified in HA-FAM134B$^+$ and HA-TEX264$^+$ HeLa cells after 6 h of culturing (Figure 8). By contrast, no red fluorescence was observed in wild type HeLa cells at 6 h postincubation (Figure 8A). Red signals in cells overexpressing FAM134B or HA-TEX264 over wild type cells were also verified by flow cytometric analysis (Figure 8B). Reticulophagy boosted by both overexpressed reticulophagic receptors is consistent with previous observations.[9,13,14] Combined, the fidelity of ER-Green-proRed to reticulophagy was further established by (1) loss of red fluorescence caused by CQ that inhibits fusion of autophagosomes with lysosomes and (2) enhanced fluorescence upon overexpression of reticulophagic receptors.

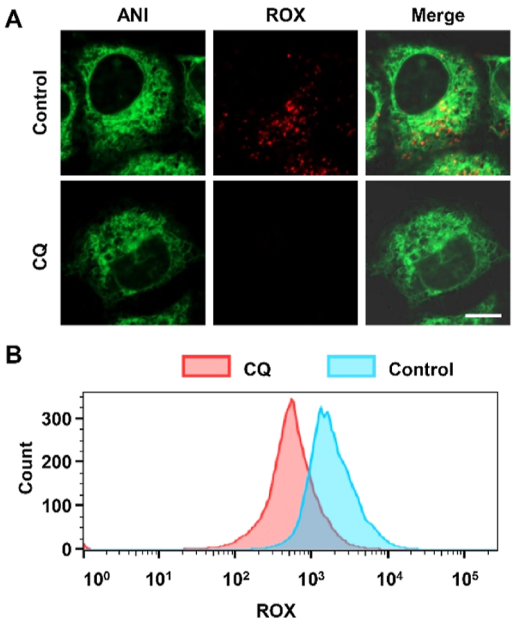

Figure 7. Inhibited ER-Green-proRed activation in cell starvation by blockade on autophagosomal fusion with lysosomes. HeLa cells prestained with ER-Green-proRed (10 μM, 1 h) were incubated for 5 h in HBSS supplemented with CQ (10 μM) or no addition (control). These cells were analyzed by confocal microscopy (A) or flow cytometry (B) for intracellular green and red fluorescence. Scale bar: 10 μm.

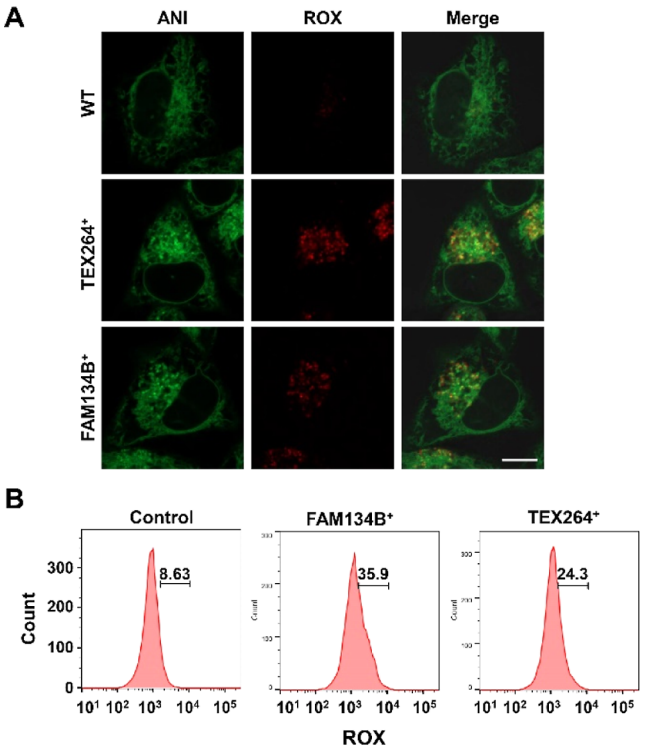

Figure 8. Boosted fluorescence activation of ER-Green-proRed in basal reticulophagy by overexpressed reticulophagic receptors. Wild type (control), HA-FAM134B$^+$, or HA-TEX264$^+$ HeLa cells were incubated with ER-Green-proRed (10 μM) for 1 h at 37 °C, incubated in fresh DMEM for 6 h, and then analyzed by confocal microscopy (A) or flow cytometry (B). Flow cytometric assays were performed using λ_{ex} = 561 nm and λ_{em} = 571−601 nm for red fluorescence, n = 10,000. Scale bars: 10 μm.

Detection of Reticulophagy Induced by Pharmacological Compounds. Pharmacological inducers of reticulophagy are of potential to treat ER stress-related diseases, as reticulophagy mediates selective elimination of the damaged ER. Because cell stress could trigger autophagy, we are interested to examine classical cell stressors for their effects on reticulophagy. Therefore, HeLa cells were treated with cyclopiazonic acid (CPA), etoposide, thapsigargin, oligomycin, rapamycin, sodium butyrate, or cisplatin (a chemotherapeutic anticancer drug) for 24 h. These cells were washed to remove extracellular agents and then analyzed with ER-Green-proRed for intracellular red fluorescence. No red signals could be observed in cells treated with thapsigargin or CPA (Figure 9), two ER stressors that activate the unfolded protein response (UPR),[15,65,66] showing their incapability to induce reticulophagy. In addition, rapamycin and oligomycin are also incompetent to elicit reticulophagy (Figure 9); the former inhibits mTORC1[67,68] and the latter inhibits ATP synthase in the mitochondria. In contrast, obvious red signals were generated in cells treated with cisplatin, etoposide, or sodium butyrate (Figure 9), three agents that, in common, could damage DNA and induce cell senescence thereof.[69−77] The observations on reticulophagy induced by DNA-damaging agents but not ER stressors suggest intricate roles of different cell stressors in ER catabolism. Taken together, these data show the feasibility of ER-Green-proRed to screen or evaluate reticulophagy-inducing pharmacological compounds.

CONCLUSIONS

Aberrant reticulophagy has been linked to diverse pathological disorders. Herein, we reported imaging of reticulophagy with

https://doi.org/10.1021/acs.analchem.3c02016
Anal. Chem. 2023, 95, 11499−11509

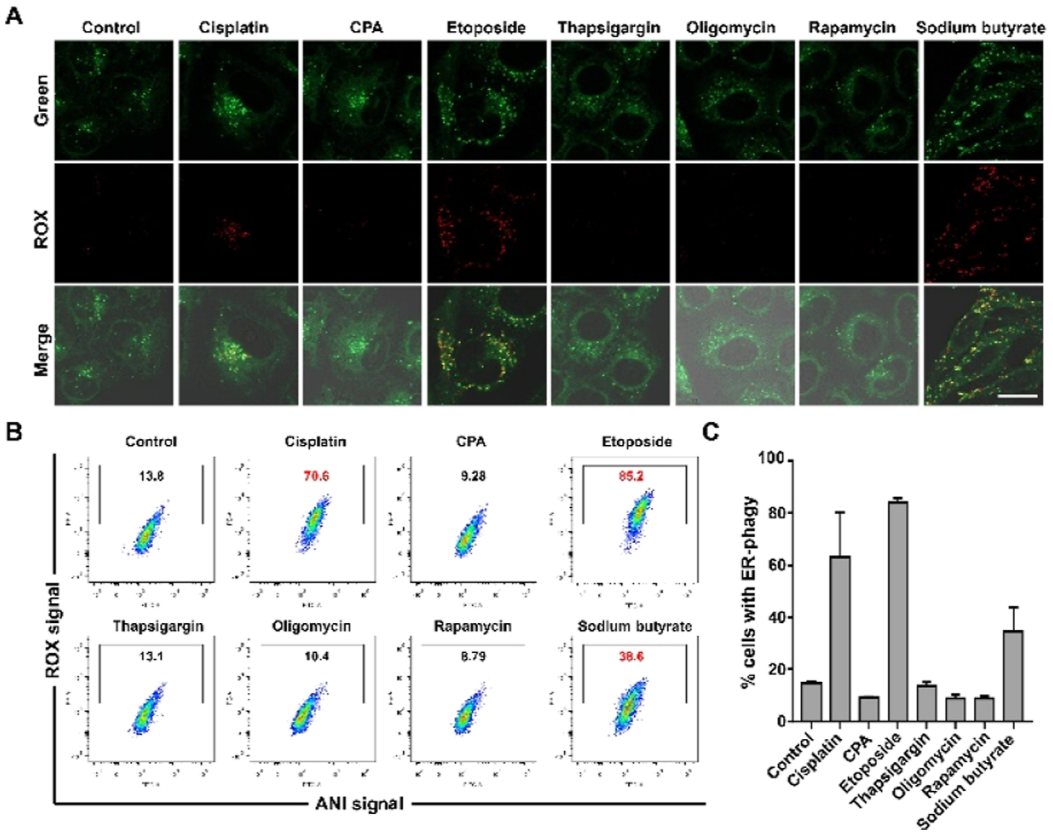

Figure 9. Discernment of reticulophagy induced by pharmacological compounds with ER-Green-proRed. MCF-7 cells were treated with cisplatin (10 μM), CPA (10 μM), etoposide (10 μM), thapsigargin (1 μM), oligomycin (4 μM), rapamycin (3 μM), sodium butyrate (10 mM), or no addition (control) for 24 h in DMEM. These cells were further cultured with ER-Green-proRed (10 μM, 1 h), washed with PBS three times, and then maintained in fresh DMEM for 6 h prior to analysis by confocal microscopy (A) and flow cytometry (B−C). Mean ± SD, $n = 3$. *, $P = 0.0205$. **, $P = 0.008$. ****, $P < 0.0001$ (t-test). Scale bars: 20 μm.

ER-Green-proRed, a synthetic diad probe composed of 3,5-trifluoromethylbenzene-conjugated naphthalimide for ER tracking and rhodamine-lactam prone to red fluorescence in acidic lysosomes. Strictly accumulated in the ER to give green fluorescence, ER-Green-proRed exhibits triggered red fluorescence upon codelivery with the ER subdomain into lysosomes, enabling sensitive imaging of reticulophagy induced by starvation, reticulophagic receptors, and pharmacological agents. These results show that functionalized ER-trackers fluorogenic to lysosomal acidity, as exemplified by ER-Green-proRed, offer a simplified and robust tool for sensitive imaging of reticulophagy and evaluation of pharmacological inducers of reticulophagy.

■ ASSOCIATED CONTENT

Supporting Information

The Supporting Information is available free of charge at https://pubs.acs.org/doi/10.1021/acs.analchem.3c02016.

Synthesis and spectral analysis of new compounds, synthetic route for ER-Green, Bz-ANI, and ER-Green-prRed, photostability and retention of the probe, imaging of reticulophagy in additional cell lines with ER-Green-prRed, and cytotoxicity of probes (PDF)

■ AUTHOR INFORMATION

Corresponding Author

Shoufa Han − *Department of Chemical Biology, College of Chemistry and Chemical Engineering, State Key Laboratory for Physical Chemistry of Solid Surfaces, the Key Laboratory for Chemical Biology of Fujian Province, the MOE Key Laboratory of Spectrochemical Analysis & Instrumentation, Xiamen University, Xiamen 361005, China;* orcid.org/0000-0002-2057-0559; Email: shoufa@xmu.edu.cn

Authors

Xiaoxue Zou − *Department of Chemical Biology, College of Chemistry and Chemical Engineering, State Key Laboratory for Physical Chemistry of Solid Surfaces, the Key Laboratory for Chemical Biology of Fujian Province, the MOE Key Laboratory of Spectrochemical Analysis & Instrumentation, Xiamen University, Xiamen 361005, China*

Yilong Shi − *State Key Laboratory of Cellular Stress Biology, Innovation Center for Cell Signaling Network, School of Life Sciences, Xiamen University, Xiamen 361005, China*

Shuo Zhang − *Department of Chemical Biology, College of Chemistry and Chemical Engineering, State Key Laboratory for Physical Chemistry of Solid Surfaces, the Key Laboratory for Chemical Biology of Fujian Province, the MOE Key Laboratory of Spectrochemical Analysis & Instrumentation, Xiamen University, Xiamen 361005, China*

Jialiang Quan − *Department of Chemical Biology, College of Chemistry and Chemical Engineering, State Key Laboratory for Physical Chemistry of Solid Surfaces, the Key Laboratory for Chemical Biology of Fujian Province, the MOE Key Laboratory of Spectrochemical Analysis & Instrumentation, Xiamen University, Xiamen 361005, China*

Jiahuai Han − *State Key Laboratory of Cellular Stress Biology, Innovation Center for Cell Signaling Network, School of Life Sciences, Xiamen University, Xiamen 361005, China*

Complete contact information is available at: https://pubs.acs.org/10.1021/acs.analchem.3c02016

Author Contributions

[§]X.Z. and Y.S. contributed equally.

Notes

The authors declare no competing financial interest.

■ ACKNOWLEDGMENTS

This work was supported by grants from the NSFC (22177096), the National Key R&D Program of China (2020YFA0803500), and the CAMS Innovation Fund for Medical Science (2019-I2M-5-062). We thank Narong Yang for helpful discussion.

■ REFERENCES

(1) Schwarz, D. S.; Blower, M. D. *Cell. Mol. Life Sci.* **2016**, *73*, 79−94.
(2) Yang, M.; Luo, S.; Wang, X.; Li, C.; Yang, J.; Zhu, X.; Xiao, L.; Sun, L. *Front. Cell Dev. Biol.* **2021**, *9*, 684526.
(3) He, L.; Qian, X.; Cui, Y. *Cells* **2021**, *10*, 2328.
(4) Wilkinson, S. *FEBS J.* **2019**, *286*, 14932−2663.
(5) Chino, H.; Mizushima, N. *Trends Cell Biol.* **2020**, *30*, 384−398.
(6) Reggiori, F.; Molinari, M. *Physiol. Rev.* **2022**, *102*, 1393−1448.
(7) Frank, M.; Duvezin-Caubet, S.; Koob, S.; Occhipinti, A.; Jagasia, R.; Petcherski, A.; Ruonala, M. O.; Priault, M.; Salin, B.; Reichert, A. S. *Biochim. Biophys. Acta* **2012**, *1823*, 2297−2310.
(8) Anding, A. L.; Baehrecke, E. H. *Dev. Cell* **2017**, *41*, 10−22.
(9) Ferro-Novick, S.; Reggiori, F.; Brodsky, J. L. *Trends Biochem. Sci.* **2021**, *46*, 630−639.
(10) Liang, J. R.; Lingeman, E.; Luong, T.; Ahmed, S.; Muhar, M.; Nguyen, T.; Olzmann, J. A.; Corn, J. E. *Cell* **2020**, *180*, 1160−1177.e20.
(11) Chen, Q.; Xiao, Y.; Chai, P.; Zheng, P.; Teng, J.; Chen, J. *Curr. Biol.* **2019**, *29*, 846−855.e6.
(12) Grumati, P.; Morozzi, G.; Hölper, S.; Mari, M.; Harwardt, M.-L. I. E.; Yan, R.; Müller, S.; Reggiori, F.; Heilemann, M.; Dikic, I. *Elife* **2017**, *6*, No. e25555.
(13) Khaminets, A.; Heinrich, T.; Mari, M.; Grumati, P.; Huebner, A. K.; Akutsu, M.; Liebmann, L.; Stolz, A.; Nietzsche, S.; Koch, N.; et al. *Nature* **2015**, *522*, 354−358.
(14) Chino, H.; Hatta, T.; Natsume, T.; Mizushima, N. *Mol. Cell* **2019**, *74*, 909−921.e6.
(15) Fumagalli, F.; Noack, J.; Bergmann, T. J.; Cebollero, E.; Pisoni, G. B.; Fasana, E.; Fregno, I.; Galli, C.; Loi, M.; Soldà, T.; et al. *Nat. Cell Biol.* **2016**, *18*, 1173−1184.
(16) Wang, L.; Liu, L.; Qin, L.; Luo, Q.; Zhang, Z. *Sci. China Life Sci.* **2017**, *60*, 333−344.
(17) Mizushima, N.; Murphy, L. O. *Trends Biochem. Sci.* **2020**, *45*, 1080−1093.
(18) Otomo, T.; Yoshimori, T. *Methods Mol. Biol.* **2017**, *1594*, 141−149.
(19) Iwashita, H.; Torii, S.; Nagahora, N.; Ishiyama, M.; Shioji, K.; Sasamoto, K.; Shimizu, S.; Okuma, K. *ACS Chem. Biol.* **2017**, *12*, 2546−2551.
(20) Li, X.; Hu, Y.; Li, X.; Ma, H. *Anal. Chem.* **2019**, *91*, 11409−11416.
(21) Shi, Y.; Zou, X.; Wen, S.; Gao, L.; Li, J.; Han, J.; Han, S. *Autophagy* **2021**, *17*, 3475−3490.
(22) Zhang, W.; Kwok, R. T.; Chen, Y.; Chen, S.; Zhao, E.; Yu, C. Y.; Lam, J. W.; Zheng, Q.; Tang, B. Z. *Chem. Commun.* **2015**, *51*, 9022−9025.
(23) Katayama, H.; Hama, H.; Nagasawa, K.; Kurokawa, H.; Sugiyama, M.; Ando, R.; Funata, M.; Yoshida, N.; Homma, M.; Nishimura, T.; et al. *Cell* **2020**, *181*, 1176−1187.e16.
(24) Lee, M. H.; Park, N.; Yi, C.; Han, J. H.; Hong, J. H.; Kim, K. P.; Kang, D. H.; Sessler, J. L.; Kang, C.; Kim, J. S. *J. Am. Chem. Soc.* **2014**, *136*, 14136−14142.
(25) McWilliams, T. G.; Prescott, A. R.; Allen, G. F.; Tamjar, J.; Munson, M. J.; Thomson, C.; Muqit, M. M.; Ganley, I. G. *J. Cell Biol.* **2016**, *214*, 333−345.
(26) Sun, N.; Yun, J.; Liu, J.; Malide, D.; Liu, C.; Rovira, I.; Holmström, K. M.; Fergusson, M. M.; Yoo, Y. H.; Combs, C. A.; et al. *Mol. Cell* **2015**, *60*, 685−696.
(27) Cheng, F.; Qiang, T.; Ren, L.; Liang, T.; Gao, X.; Wang, B.; Hu, W. *Analyst* **2021**, *146*, 2632−2637.
(28) Gui, L.; Yuan, Z.; Kassaye, H.; Zheng, J.; Yao, Y.; Wang, F.; He, Q.; Shen, Y.; Liang, L.; Chen, H. *Chem. Commun.* **2018**, *54*, 9675−9678.
(29) Hou, J. T.; Ren, W. X.; Li, K.; Seo, J.; Sharma, A.; Yu, X. Q.; Kim, J. S. *Chem. Soc. Rev.* **2017**, *46*, 2076−2090.
(30) Li, M.; Huang, Y.; Song, S.; Shuang, S.; Dong, C. *ACS Appl. Bio Mater.* **2022**, *5*, 2777−2785.
(31) Li, X.; Liang, X.; Yin, J.; Lin, W. *Chem. Soc. Rev.* **2021**, *50*, 102−119.
(32) Liu, Y.; Teng, L.; Chen, L.; Ma, H.; Liu, H. W.; Zhang, X. B. *Chem. Sci.* **2018**, *9*, 5347−5353.
(33) Liu, Y.; Zhou, J.; Wang, L.; Hu, X.; Liu, X.; Liu, M.; Cao, Z.; Shangguan, D.; Tan, W. *J. Am. Chem. Soc.* **2016**, *138*, 12368−12374.
(34) Munan, S.; Ali, M.; Yadav, R.; Mapa, K.; Samanta, A. *Anal. Chem.* **2022**, *94*, 11633−11642.
(35) Munan, S.; Kottarathil, S.; Joseph, M. M.; Jana, A.; Ali, M.; Mapa, K.; Maiti, K. K.; Samanta, A. *ACS Sens.* **2022**, DOI: 10.1021/acssensors.1c02381.
(36) Niu, L. Q.; Huang, J.; Yan, Z. J.; Men, Y. H.; Luo, Y.; Zhou, X. M.; Wang, J. M.; Wang, J. H. *Spectrochim. Acta, Part A* **2019**, *207*, 123−131.
(37) Tang, W.; Dai, Y.; Gu, B.; Liu, M.; Yi, Z.; Li, Z.; Zhang, Z.; He, H.; Zeng, R. *Analyst* **2020**, *145*, 1427−1432.
(38) Wang, H.; Hu, J.; Yang, G.; Zhang, X.; Zhang, R.; Uvdal, K.; Zhang, Z.; Wu, X.; Hu, Z. *Sens. Actuators, B* **2020**, *320*, 128418.
(39) Wang, T. R.; Chen, Q.; Tang, M. Y.; Zhang, Y.; Shen, S. L.; Cao, X. Q. *Spectrochim. Acta, Part A* **2022**, *280*, 121496.
(40) Wen, S.; Hu, X.; Shi, Y.; Han, J.; Han, S. *Anal. Chem.* **2021**, *93*, 16887−16898.
(41) Xia, S.; Wang, J.; Zhang, Y.; Whisman, N.; Bi, J.; Steenwinkel, T. E.; Wan, S.; Medford, J.; Tajiri, M.; Luck, R. L.; et al. *J. Mater. Chem. B* **2020**, *8*, 1603−1615.
(42) Yue, Y.; Huo, F.; Lee, S.; Yin, C.; Yoon, J. *Analyst* **2017**, *142*, 30−41.
(43) Zhang, D.; He, Y.; Wang, J.; Wu, L.; Liu, B.; Cai, S.; Li, Y.; Yan, W.; Yang, Z.; Qu, J. *J. Biophot.* **2022**, *15*, No. e202200006.
(44) Fang, H.; Hu, L.; Chen, Q.; Geng, S.; Qiu, K.; Wang, C.; Hao, M.; Tian, Z.; Chen, H.; Liu, L.; et al. *Biomaterials* **2023**, *292*, 121929.
(45) He, Y.; Shin, J.; Gong, W.; Das, P.; Qu, J.; Yang, Z.; Liu, W.; Kang, C.; Qu, J.; Kim, J. S. *Chem. Commun.* **2019**, *55*, 2453−2456.
(46) Shi, Y.; Zou, X.; Zheng, X.; Wu, Y.; Han, J.; Han, S. *Autophagy* **2023**, *17*, 2015−2025.
(47) Silswal, A.; Koner, A. L. *Chem. Commun.* **2023**, *59*, 1769−1772.
(48) Man, H.; Bian, H.; Zhang, X.; Wang, C.; Huang, Z.; Yan, Y.; Ye, Z.; Xiao, Y. *Biosens. Bioelectron.* **2021**, *189*, 113378.
(49) Liu, C.; Zhou, L.; Xie, L.; Zheng, Y.; Man, H.; Xiao, Y. *Chin. Chem. Lett.* **2022**, *33*, 2537−2540.
(50) Xue, Z.; Zhao, H.; Liu, J.; Han, J.; Han, S. *ACS Sens.* **2017**, *2*, 436−442.
(51) Xue, Z.; Zhao, H.; Liu, J.; Han, J.; Han, S. *Chem. Sci.* **2017**, *8*, 1915−1921.
(52) Dadina, N.; Tyson, J.; Zheng, S.; Lesiak, L.; Schepartz, A. *Curr. Opin. Chem. Biol.* **2021**, *65*, 154−162.
(53) Danylchuk, D. I.; Jouard, P. H.; Klymchenko, A. S. *J. Am. Chem. Soc.* **2021**, *143*, 912−924.
(54) Fujisawa, A.; Tamura, T.; Yasueda, Y.; Kuwata, K.; Hamachi, I. *J. Am. Chem. Soc.* **2018**, *140*, 17060−17070.
(55) Ghosh, S.; Nandi, S.; Ghosh, C.; Bhattacharyya, K. *Chemphyschem* **2016**, *17*, 2777−2823.

(56) Gong, S.-S.; Chen, L.-L.; Du, K.; Yin, Y.; Yang, R.-X.; Shi, R.; Peterson, B.-R.; Feng, F.; Sun, Q. *Chemistry* **2023**, *29*, No. e202300315.
(57) Goujon, A.; Colom, A.; Strakova, K.; Mercier, V.; Mahecic, D.; Manley, S.; Sakai, N.; Roux, A.; Matile, S. *J. Am. Chem. Soc.* **2019**, *141*, 3380−3384.
(58) Ma, H.; Lu, Y.; Huang, Z.; Long, S.; Cao, J.; Zhang, Z.; Zhou, X.; Shi, C.; Sun, W.; Du, J.; et al. *J. Am. Chem. Soc.* **2022**, *144*, 3477−3486.
(59) Meinig, J. M.; Fu, L.; Peterson, B. R. *Angew. Chem. Int. Ed.* **2015**, *54*, 9696−9699.
(60) Wagner, N.; Stephan, M.; Hoglinger, D.; Nadler, A. *Angew. Chem., Int. Ed.* **2018**, *57*, 13339−13343.
(61) CellLight. *ER-RFP, BacMam 2.0, C10591, Thermo Fisher Scientific*. (accessed April 22 2022). https://www.thermofisher.cn/order/catalog/product/C10591#/C10591.
(62) Harada, M.; Shakado, S.; Sakisaka, S.; Tamaki, S.; Ohishi, M.; Sasatomi, K.; Koga, H.; Sata, M.; Tanikawa, K. *Liver* **2008**, *17*, 244−250.
(63) Mauthe, M.; Orhon, I.; Rocchi, C.; Zhou, X.; Luhr, M.; Hijlkema, K. J.; Coppes, R. P.; Engedal, N.; Mari, M.; Reggiori, F. *Autophagy* **2018**, *14*, 1435−1455.
(64) Hübner, C. A.; Dikic, I. *Cell Death Differ.* **2020**, *27*, 833−842.
(65) Wu, S.; Li, Z.; Han, J.; Han, S. *Chem. Commun.* **2011**, *47*, 11276−11278.
(66) Abdullahi, A.; Stanojcic, M.; Parousis, A.; Patsouris, D.; Jeschke, M. G. *Shock* **2017**, *47*, 506−513.
(67) Rangaraju, S.; Verrier, J. D.; Madorsky, I.; Nicks, J.; Dunn, W. A., Jr.; Notterpek, L. *J. Neurosci.* **2010**, *30*, 11388−11397.
(68) Edwards, S. R.; Wandless, T. J. *J. Biol. Chem.* **2007**, *282*, 13395−13401.
(69) te Poele, R. H.; Okorokov, A. L.; Jardine, L.; Cummings, J.; Joel, S. P. *Cancer Res.* **2002**, *62*, 1876−1883.
(70) Terao, Y.; Nishida, J.; Horiuchi, S.; Rong, F.; Ueoka, Y.; Matsuda, T.; Kato, H.; Furugen, Y.; Yoshida, K.; Kato, K.; et al. *Int. J. Cancer* **2001**, *94*, 257−267.
(71) Xiao, H.; Hasegawa, T.; Miyaishi, O.; Ohkusu, K.; Isobe, K. *Biochem. Biophys. Res. Commun.* **1997**, *237*, 457−460.
(72) Petrova, N. V.; Velichko, A. K.; Razin, S. V.; Kantidze, O. L. *Aging Cell* **2016**, *15*, 999−1017.
(73) Litwiniec, A.; Gackowska, L.; Helmin-Basa, A.; Żuryń, A.; Grzanka, A. *Cancer Cell Int.* **2013**, *13*, 9.
(74) Probin, V.; Wang, Y.; Bai, A.; Zhou, D. *J. Pharmacol. Exp. Ther.* **2006**, *319*, 551−560.
(75) Qu, K.; Lin, T.; Wang, Z.; Liu, S.; Chang, H.; Xu, X.; Meng, F.; Zhou, L.; Wei, J.; Tai, M.; et al. *Front. Med.* **2014**, *8*, 227−235.
(76) Veena, M. S.; Wilken, R.; Zheng, J. Y.; Gholkar, A.; Venkatesan, N.; Vira, D.; Ahmed, S.; Basak, S. K.; Dalgard, C. L.; Ravichandran, S.; et al. *J. Biol. Chem.* **2014**, *289*, 34921−34937.
(77) Wang, X.; Wong, S. C.; Pan, J.; Tsao, S. W.; Fung, K. H.; Kwong, D. L.; Sham, J. S.; Nicholls, J. M. *Cancer Res.* **1998**, *58*, 5019−5022.

https://doi.org/10.1021/acs.analchem.3c02016
Anal. Chem. 2023, 95, 11499−11509